Expandable N-Legged Converter to Drive Closely Spaced Multitransmitter Wireless Power Transfer Systems for Dynamic Charging

Farzad Farajizadeh, *Student Member, IEEE*, D. Mahinda Vilathgamuwa, *Senior Member, IEEE*, Dejan Jovanovic, *Member, IEEE*, Prasad Jayathurathnage, *Member, IEEE*, Gerard Ledwich, *Senior Member, IEEE*, and Udaya Madawala, *Fellow, IEEE*

***Abstract*—Expandable and flexible wireless power transfer (WPT) systems have been in demand in numerous industry applications, especially for dynamic chargers in electric vehicles. Those systems, however, bring about certain technical issues such as modulation technique and topology of the transmitter side, and transferred power profile of the transmitters. In this article, a new converter topology to drive closely spaced segmented dynamic wireless power transfer (DWPT) systems is proposed. The proposed converter can be expanded to cater for different number of transmitters, and it can provide a uniform transferred power profile throughout the path of transmitter coils, known as track. Furthermore, this article focuses on analyzing the operation of the converter and the effect of closely spaced transmitters over its operation. To show the effectiveness of the proposed topology and its modulation technique, the converter is simulated and experimentally tested using a laboratory prototype. The results are compared and analyzed, and their close agreement shows the validity of the proposed technique.**

***Index Terms*—Coordination factor, cross coupling, electric vehicles (EV), expandable wireless power transfer (WPT) system, inductive charging, magnetic profile, mode changing transients, multitransmitter wireless power transfer systems, transferred power profile.**

I. Introduction

AMONGST all carbon emitting contributors, fossil fuel vehicles have a significant influence on air pollution. The use of electric vehicles (EVs) is one of the most effective solutions to address this issue [1], [2]. EVs still find it difficult competing against their fossil fuel counterparts, especially in terms of power and energy density [1]. The placement of higher number of accessible electric chargers along the way can be seen as a sensible approach [3]. However, wired chargers are stationary and the vehicles must stop at the charging station to get charged [4], the mechanical connectors need to be serviced regularly [5], and they are not completely safe in wet or dirty environments [6]. As an alternative, wireless charging can solve these issues. Wireless charging process can be done either stationary, while the EV is stopped, or dynamically, while it is on the move [7]. However, the use of dynamic chargers is more advantageous as they save the driver's time. Furthermore, dynamic wireless power transfer (DWPT) increases the driver's safety, enhances the reliability of the system, and decreases the maintenance costs, as it does not need any mechanical connectors for charging [8].

Transmitters in DWPT systems can be divided into two main categories of elongated transmitters and segmented transmitters [9]. In the elongated type, a long coil acts as the transmitter, which is laid along the track. However, in this method, the magnetic flux produced by the transmitter is not confined, and the ratio between linkage and leakage fluxes is significantly small. This leads to high electromagnetic interferences and a high level of electromagnetic exposure from the noninteractive parts of the transmitter. In terms of electric concerns, power losses in the noninteractive part of the transmitter and the size of compensators and power supplies to drive the transmitter are the main drawbacks of the elongated transmitter [4], [10]–[15]. Moreover, the reliability of the system is dependent on the length of the transmitter, and in case of any failure, all the length of coverage would malfunction.

In the other method of DWPT, i.e., in segmented transmitters, several transmitters are deployed in a track, and they can be driven by one or more than one converter [10]. This method addresses the issues of undesirable losses and exposure in noninteractive parts [4], [11], [16], electromagnetic interferences [4], [12], and high ratings of drivers and compensators [12], [14]. However, making a uniform transferred power profile is not easily achievable, and if transmitters are not closely spaced, the linkage flux would be even less than that of the elongated type [11], [16]–[18].

To expand and refine the transferred power profile, Budhia *et al.* [6] have established the concept of double windings, also known as DD windings, on the track side, which are magnetically connected in series and electrically connected in parallel. This approach not only expands the coverage of transmitter magnetic field, but also removes the power null

Manuscript received February 15, 2019; revised June 19, 2019; accepted August 12, 2019. Date of publication September 8, 2019; date of current version January 10, 2020. Recommended for publication by Associate Editor R. Hui. *(Corresponding author: Farzad Farajizadeh.)*

F. Farajizadeh, D. M. Vilathgamuwa, D. Jovanovic, and G. Ledwich are with the Department of Electrical Engineering and Computer Science, Queensland University of Technology, Brisbane, QLD 4001, Australia (e-mail: f.faradjizadeh@gmail.com; mahinda.vilathgamuwa@qut.edu.au; dejan.jovanovic@qut.edu.au; g.ledwich@qut.edu.au).

P. Jayathurathnage is with the Department of Electronics and Nanoengineering, School of Electrical Engineering, Aalto University, Espoo 00076, Finland (e-mail: prasad.jayathurathnage@aalto.fi).

U. Madawala is with the Department of Electrical Computer Engineering, The University of Auckland, Auckland 92019, New Zealand (e-mail: u.madawala@auckland.ac.nz).

Color versions of one or more of the figures in this article are available online at http://ieeexplore.ieee.org.

Digital Object Identifier 10.1109/TPEL.2019.2939848

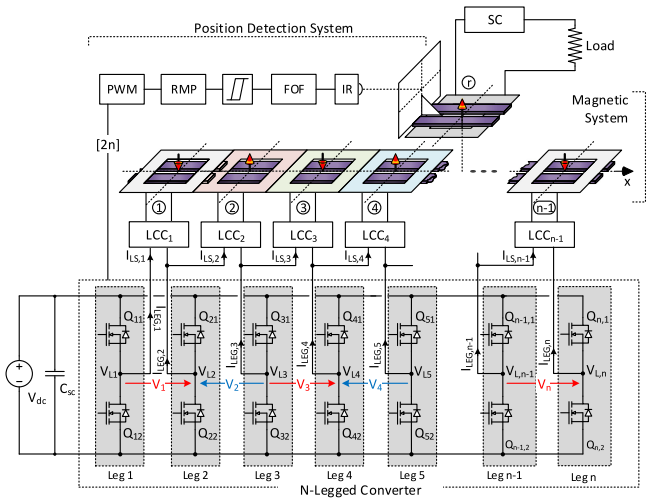

Fig. 1. Generic view of NLC driving a segmented DWPT. In this figure, RMP stands for ramp controller, FOF is used for the first order filter, IR stands for infrared sensor, SC is series compensator, and LCC is the type of compensators used in the transmitters.

between DD transmitters. To remove the power null, in addition to DD windings, another quadrature winding, known as Q winding, is also used on the pickup side.

To develop the DDQ concept into an expandable pattern, the work presented in [12] and [19] uses adjacent multiple DD transmitters and drive them in parallel through an H-bridge converter. While this approach is successful in expanding the transferred power profile along the pickup direction, currents in all transmitters are almost equal and cannot be controlled individually, and that results in undesirable power losses in non-interactive transmitters. The lack of controllability in transmitter currents can also lead to power profile fluctuations, which make power tracking difficult in the pickup side.

In [20], a comprehensive study over magnetic profiles of different types of DDQ topologies, especially when coils are driven independently, is carried out. However, the effect of cross coupling amongst the adjacent transmitters on the driving converters is not studied. To tackle this problem, the work presented in [2] uses individually driven DD coils with a specific arrangement to make a uniform transferred power profile. In this method, however, the cross coupling between transmitters prevents the close positioning of the transmitters, and consequent spacing of transmitters cannot effectively contribute to alleviate the bumps of transferred power. In all of these DD(/Q) based methods, although the smart approach of using Q winding improves the power profile of the system, excessive use of wires and ferrites, and the lack of controllability in each transmitter (each of D or Q windings) are two weak points of this approach.

In [21], a multileg inverter is proposed to provide a more economical arrangement to drive dynamic wireless systems for EV applications. However, enhancement of transferred power profile, soft switching, and mode changing transients has not been studied, as the main concern of this article was load detection.

Therefore, taking the advantage of a refined LCC compensator introduced in [22], an expandable N-legged converter (NLC) is proposed to drive a closely spaced segmented DWPT system, as shown in Fig. 1. The resultant system is capable of making a uniform power profile for the pickup at a high efficiency. This can be achieved with a reduced number of power electronic switches in the driving system and a less volume of copper and ferrite in the magnetic system compared to the conventional systems. A brief comparison of the proposed converter with the conventional DDQ system is presented in [23]. In this article, a more in-depth study is done on the effect of cross couplings amongst the transmitters, and transition between different modes of operation. Furthermore, the system is experimentally built and tested.

The proposed converter consists of n legs that can individually drive the coils with a reduced number of switches to form a desirable transferred power profile. Moreover, based on the method proposed in [22], a refined compensator that can mitigate the undesirable effect of cross coupling in the transmitters is used. In the process of achieving a desirable transferred power profile, different modes of operation are defined for NLC and they are changed with the position of the pickup. As shown in Fig. 1, the pickup position must be sensed and sent to the driving system. So far, studies have shown some promising results in the realm of pickup position estimation by directly measuring WPT coil-compensator current and voltages [24]–[27], or with the use of additional sensing systems [28], [29], and yet some more accurate and fast techniques are being investigated. Position estimation is important particularly in EVs to make them smarter, especially for auto piloting. With the use of some of these sensors and communication links between them and the WPT transmitters deployed on the road, accurate detection of the pickup position is not that a far-fetched preposition. However, as the estimation of the pickup position is not the main concern of this article, a simple infrared sensor is used to detect the position of the pickup and a gradual change of modes with the knowledge of system parameters is adopted to mitigate the mode changing transients. Owing to the presence of multiple legs in the NLC, the converter possesses a remarkable reliability and tolerance against faults, and this aspect is to be comprehensively studied in a subsequent work.

Fig. 1 shows a generic view of the proposed system studied in this article. The expandable converter is presented in Section II. The converter drives a closely spaced magnetic system, consisting of $n-1$ transmitters and one receiver (r).

The magnetic system is studied in Section III. The transmission of power from the NLC to the transmitters is done through the refined LCC compensators, comprising of an inductor, two capacitors, and a coupled inductor, which is explained in detail in Section IV. Pickup position is detected by a position detection system comprising of an infrared sensor, a first order filter, a hysteresis controller, a ramp filter, and a pulsewidth modulation signal generator. The mode changing strategy to suppress undesirable transients is proposed in Section V.

To validate the mathematical concepts, the system is simulated based on the specifications given in Table I by ANSYS Electronics Desktop/Maxwell [30] and MATLAB/Simscape/Fundamental Blocks/Power Electronics [31], and the results are shown in the respective sections. Moreover, experiments are conducted for further validation of the proposed concept, and corresponding experimental results are given in Section VII.

II. Operation of the Converter

To drive a multitransmitter segmented DWPT system effectively, the maintenance of transferred power quality and efficiency is of prime concern. This can be addressed by closely spacing the transmitters in the system (as explained in

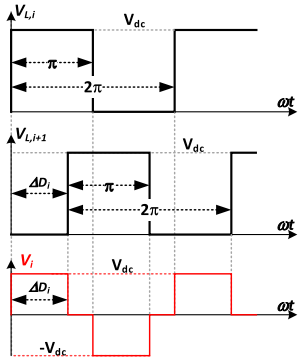

Fig. 2. Leg-to-ground and leg-to-leg voltages of two adjacent legs.

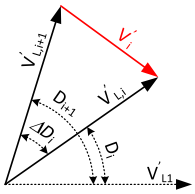

Fig. 3. Voltage phasor diagram of leg-to-ground ($V_{\mathrm{L},i}$) and leg-to-leg (V_i) fundamentals of adjacent legs in an NLC ($V'_{\mathrm{L},i}$ is the fundamental component of $V_{\mathrm{L},i}$).

Section III) and by appropriately exciting the transmitters corresponding to the pickup position. To enhance the efficiency, the transmitters, which are not effectively coupled with the pickup, should be turned OFF. For this purpose, the flow of power in each transmitter must be controlled. In this section, a new converter with a low number of power electronic switches is presented to serve this purpose.

As shown in Fig. 1, the proposed converter comprises of n number of legs, which are connected in parallel, and they can form $n-1$ pairs of adjacent output terminals. The output terminals can be used to drive an expandable segmented DWPT system. The control parameter to change the output voltage is the difference of voltage phase angles in two adjacent legs, represented as $\Delta D_i = D_{i+1} - D_i$. Therefore, the converter can change its output leg-to-leg voltage of V_i according to (1). Fig. 2 shows the waveforms of leg-to-ground and leg-to-leg voltages of two adjacent legs, and Fig. 3 depicts the voltage phasors of the leg-to-ground and leg-to-leg fundamentals

$$V_i = \underbrace{\frac{2}{\pi} V_{\mathrm{dc}} \sin\left(\frac{D_{i+1} - D_i}{2}\right)}_{V_m} \angle \underbrace{\left(\frac{D_{i+1} + D_i}{2} - \frac{\pi}{2}\right)}_{\theta} \tag{1}$$

where V_m and θ are the amplitude and phase angle of V_i respectively.

In segmented DWPT systems, the maximum transferred power occurs when the magnetic fields of all transmitters are in the same phase and the same magnetic polarity. This is similar to the summation of many vectors, which will reach the maximum value when all the vectors are aligned and in the same direction [32], [33]. In the proposed converter, the maximum output voltage of two adjacent pair of terminals occurs when their phase angles are 180° out of phase, as shown in Fig. 3. Therefore, to make two identically wound coils produce their maximum magnetic fields along the same direction, the terminals of every other coil must be flipped when they are connected to the NLC output terminals.

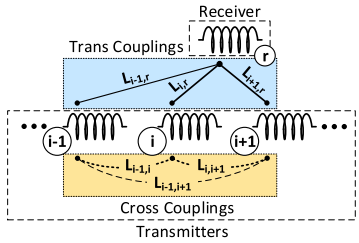

Fig. 4. Couplings in a segmented DWPT system.

As an example, assuming that in the multitransmitter DWPT system shown in Fig. 1, transmitter i is at its desirable coupling level, by applying $\Delta D_i = D_{i+1} - D_i = 180^\circ$ or -180° to the phase angle between legs i and $i+1$, transmitter i can have the highest voltage, and as a result it can transfer the highest power to the pickup. Meanwhile, for other transmitters where the coupling level is low, the phase angle between their corresponding adjacent legs in the NLC should be kept zero to turn OFF the transmitters such that unnecessary losses are prevented. Similar analogy can be used to explain when two (i and $i+1$) or more (e.g., i, $i+1$, and $i+2$) transmitters have a desirable coupling with the pickup at a time. In those cases, the converter can provide the interacted coils with the maximum voltage and turn OFF the other ones ($\Delta D_i = 180^\circ$, $\Delta D_{i+1} = -180^\circ$, for two interactive coils, and in case of involvement of the third coil $\Delta D_{i+2} = 180^\circ$).

How to define the modes of operation in a regularly distributed multitransmitter segmented DWPT and to use NLC to drive the DWPT system is explained in the following sections.

III. Trans Coupling and Magnetic Coordination

As shown in Fig. 4, in segmented DWPT systems, there are different types of couplings that take place while the system operates. In terms of transferred power, the desirable couplings are the ones that occur between transmitters and receivers, ($L_{i-1,\mathrm{r}}$, $L_{i,\mathrm{r}}$, and $L_{i+1,\mathrm{r}}$) which from here onward are defined as trans couplings. Moreover, the undesirable couplings that happen between the coils at either receiver or transmitter side ($L_{i-1,i}$, $L_{i,i+1}$, and $L_{i-1,i+1}$) and are known as cross couplings.

One of the main goals of this article is to form a uniform trans coupling profile in a segmented DWPT system as it can give rise to a uniform transferred power [23]. This is not achievable unless the transmitters are placed near to each other, which will in turn increase the cross coupling between them. The undesirable effect of the cross coupling between transmitter coils is disruption of soft switching in the driving power converters. This phenomenon creates a shift between voltage and current zero crossing transitions of the NLC switches, causing some residual current at the instant of voltage zero crossing and when switches are turned ON or turned OFF. This is also known as hard switching and will lead to a higher power loss or even thermal failure of the switches. Here, the influence of cross coupling on this current is analyzed and handled using a refined LCC compensator proposed in [22].

As shown in Fig. 4, in a segmented DWPT system with one receiver coil and multiple transmitters, the induced voltage in the coil can be expressed as follows:

$$E_n = s \sum_{i=1}^{n-1} L_{i,\mathrm{r}} I_i \tag{2}$$

where $L_{i,\mathrm{r}}$ is the trans coupling between the i^{th} transmitter and the receiver, and I_i is the i^{th} transmitter current. The induced voltage E_n is the main source of energy at the receiver side and acts as a current-controlled voltage source. This voltage is linked to the current of each transmitter through the corresponding trans coupling. Therefore, by properly designing the magnetic system and injecting appropriate current into the transmitters, a continuous profile of voltage is achievable. To have a dedicated criterion for this contribution of trans couplings and injected currents, a coordination factor χ, as given in (3a), can be defined

$$\chi = L_{1,\mathrm{r}} I_1 + L_{2,\mathrm{r}} I_2 + \cdots + L_{n-1,\mathrm{r}} I_{n-1} \tag{3a}$$

$$I_{\mathrm{r}} = \frac{\omega \chi}{R_{\mathrm{L}}} \Rightarrow P_{\mathrm{out}} = \frac{\omega^2 \chi^2}{R_{\mathrm{L}}} \tag{3b}$$

$$\eta = \frac{R_{\mathrm{L}} \omega^2 \chi^2}{(R_{\mathrm{r}} + R_{\mathrm{L}})^2 \times \sum_{i=1}^{n-1} R_i I_i^2 + R_{\mathrm{r}} \omega^2 \chi^2} \tag{3c}$$

where I_i is the current of transmitters, $L_{i,\mathrm{r}}$ is the i^{th} trans coupling, R_{L} is the resistance of the load, R_i is the i^{th} transmitter series equivalent resistance, and R_{r} is the equivalent resistance of the receiver. As $k = \omega / R_{\mathrm{L}}$ in (3b) is a constant, I_{r} has a direct relationship to the coordination factor χ. As such, the output power $P_{\mathrm{out}} = R_{\mathrm{L}} I_{\mathrm{r}}^2$ has a direct relationship to χ^2. Therefore, hereinafter, current of receiver is selected to represent the output power. Furthermore, (3c) shows that the higher the χ, the higher the efficiency of the WPT coils. In this equation, $\sum_{i=1}^{n-1} R_i I_i^2$ represents the power losses in the transmitters, and it shows if the current in uncoupled coils is limited to zero, the efficiency will increase even more. This explains why different modes of operation are defined for the proposed system.

As the optimization of magnetic system is not the primary concern of this article, transmitters and receivers are considered to be having identical dimensions with rectangular polarized structure. The parameters of coils are given in Table I. This arrangement of identical in-line transmitters is the simplest pattern that can be used, and it is expandable either along the track or across its width. If transmitters are deployed in a regular manner, based on their pattern of deployment, some limited modes of operation can be defined to excite the transmitters and obtain the highest transferred power capacity with a minimum swing regardless of the number of transmitters.

Fig. 5 shows the experimental magnetic profiles of a segmented DWPT system consisting of three transmitters (coils 1 to 3) and one receiver (r) obtained from the experimental measurements. Five main displacement positions (A, B, C, D, and E) are indicated in Fig. 5, where A, C, and E correspond to the aligned positions of transmitters 1, 2, and 3, respectively, and B and D are between transmitter pairs 1-2 and 2-3, respectively, where their mutual inductances are equal.

Here, with the use of the coordination factor, two basic modes of *single* and *overlap*, can be defined for the trans couplings. In *single* mode, only one transmitter interacts with the pickup, as shown in modes "1," "3," and "5" in Fig. 5, whereas in the *overlap* mode, two overlapped trans couplings, modes "2" and "4" in Fig. 5, with the pickup take place. For the given prototype, the pitch of transmitters is chosen so that there are two descending and incremental slopes for trans couplings for every overlapping adjacent coils seen by the receiver (r), as shown in *overlap* modes

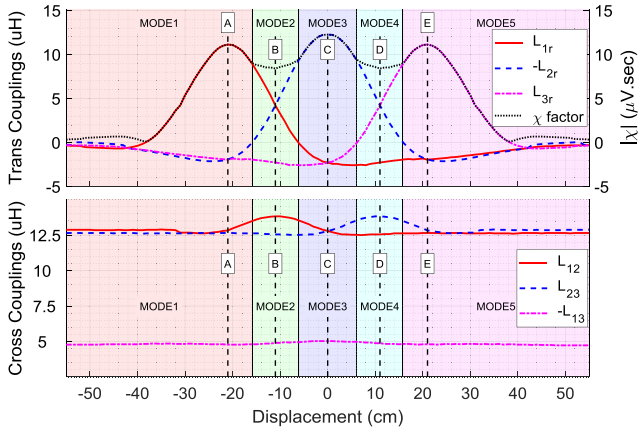

Fig. 5. Experimental results for trans couplings, coordination factor (χ), and cross coupling of a segmented DWPT system consisting of three transmitters and one receiver, based on the specifications of Table I.

of "2" and "4." A similar pattern can be replicated with the increase in the number of transmitters, as shown in Fig. 5.

As mentioned in Section II, to keep the magnetic polarity of the identically wound windings in a segmented DWPT system the same, terminals of every other coil must be flipped when they are connected to the NLC output terminals. Using this, NLC can add up the effect of resultant fields in χ. Considering this fact for the obtained magnetic profile of the segmented DWPT in Fig. 5, five modes of operation can be defined. Taking mode "2" as an example, the sequence of signs for $[L_{1,\mathrm{r}}, -L_{2,\mathrm{r}}, L_{3,\mathrm{r}}]$ can be seen as $[\oplus, \oplus, \ominus]$. Therefore, the effect of $L_{1,\mathrm{r}}$ and $L_{2,\mathrm{r}}$ can be added up by the converter with the selection of $[D_1, D_2, D_3, D_4]$ as $[0°, 180°, 0°, 0°]$ or $[180°, 0°, 180°, 180°]$ to obtain the highest possible χ in that region. Using the same analogy, different modes can be defined to obtain the highest possible χ at different pickup positions, as shown in Fig. 5. In the next section, using coupled inductors in the LCC compensator, the undesirable effect of cross coupling is addressed.

IV. Compensation

Transmitter coils of the proposed segmented DWPT system is compensated with an integrated LCC compensator with coupled inductors [22], as shown in Fig. 6. LCC compensator at its resonant frequency acts as a current source and the variation of the reflected load from the pickup side does not influence the current amplitude in the transmitters. This feature makes the LCC a desirable choice for DWPT systems [12], [34]–[36]. Current in LCC primary loop ($I_{\mathrm{LS},i}$) can be defined as

$$I_{\mathrm{LS},i} = \underbrace{\left(C_{\mathrm{P},i} L_{ii} \omega^2 - 1 - \frac{C_{\mathrm{P},i}}{C_{\mathrm{S},i}}\right) \times \left(\overbrace{j\omega C_{\mathrm{P},i} V_i}^{|I_i|}\right)}_{\substack{\text{Quadrature Term} \\ \text{(Independent)}}} + \underbrace{\left(C_{\mathrm{P},i} \omega^2 \sum_{k=1}^{n-2} L_{\mathrm{T},ii}\right) \times \left(\overbrace{j\omega C_{\mathrm{P},i} V_i}^{|I_i|}\right)}_{\substack{\text{Quadrature Term} \\ \text{(CPI Self-Inductors)}}}$$

$$
\begin{aligned}
&\underbrace{+C_{\mathrm{P},i}\omega^2 \sum_{\substack{k=1\\k\neq i}}^{n-1} L_{ki}\left(\overbrace{j\omega C_{\mathrm{P},k}V_k}^{|I_k|}\right)}_{\text{Quadrature Term (Cross Coupling)}}\\
&\underbrace{-C_{\mathrm{P},i}\omega^2 \sum_{\substack{k=1\\k\neq i}}^{n-1} L_{\mathrm{T},ki}\left(\overbrace{j\omega C_{\mathrm{P},k}V_k}^{|I_k|}\right)}_{\text{Quadrature Term (CPI Compensation)}}\\
&\underbrace{+\left(\frac{C_{\mathrm{P},i}}{Z_{\mathrm{L}}}L_{i,\mathrm{r}}^2\omega^3\right)\times\left(\overbrace{\omega C_{\mathrm{P},i}V_i}^{|I_i|}\right)}_{\text{Direct Term (Reflected Load)}}\\
&\underbrace{+\frac{C_{\mathrm{P},i}}{Z_{\mathrm{L}}}\omega^3 \sum_{\substack{k=1\\k\neq i}}^{n-1} L_{ni}L_{k,\mathrm{r}}\left(\overbrace{\omega C_{\mathrm{P},k}V_k}^{|I_k|}\right)}_{\text{Direct Term (Double Reflected Load)}}
\end{aligned}
\tag{4}
$$

where $C_{\mathrm{S},i}$, $C_{\mathrm{P},i}$, and $L_{\mathrm{S},i}$ are series capacitor, parallel capacitor, and series inductor of the LCC compensator, respectively. L_{ij} and L_{ii} are the cross coupling and self-inductance of the transmitters, $L_{\mathrm{T},ij}$ and $L_{\mathrm{T},ii}$ are the cross coupling and self-inductance of the coupled inductors, Z_{L} is the compensated load at the pickup side, and V_i is the fundamental leg-to-leg voltage of the converter. The current of the transmitter I_i is given as $I_i = -j\omega C_{\mathrm{P},i}V_{i,1}$. Although, in the experimental prototype, cross couplings of all three transmitters are compensated using coupling inductors, for a realistic expanded system of $n-1$ coils for an NLC, the compensation of cross couplings due to at most two coils neighboring the excited coil would be sufficient. This is with reference to Fig. 5 depicting the cross couplings, where it shows that further the coil away from the excited coil, lower the effect of the cross couplings as L_{12} and L_{23} are significantly higher than L_{13}, and cross couplings would be negligible for more than two coils away from the excited coil.

The simulation and theoretical waveforms of the transmitter current I_i and LCC primary loop current $I_{\mathrm{LS},i}$ are shown in Figs. 7 and 8, respectively.

The theoretical results for $I_{\mathrm{LS},i}$ are obtained as the magnitude of the phasor expressions in (4), and the results for $I_{\mathrm{LEG},i}$ and I_i can be obtained in a similar way.

As shown in Figs. 5 and 7, as pickup gets closer to the transmitter number one, $L_{1,\mathrm{r}}$ coupling starts to increase. Considering $\oplus$ and $\ominus$ for positive and negative values of trans couplings, respectively, in this mode, the trans couplings follow $[\oplus, \ominus, \ominus]$. Therefore, exciting the converter with $[180°, 0°, 0°, 0°]$ will only energize the first coil, and pickup current will start to increase and follow the χ factor, as it is expected from (3b), as it reaches the second mode. In the second mode, the converter can excite the second transmitter to improve χ, as the trans coupling sequence of signs is $[\oplus, \oplus, \ominus]$, this can be done by applying $[0°, 180°, 0°, 0°]$ to NLC legs. When the converter enters the third mode of operation, the sequence of signs in trans couplings is $[\ominus, \oplus, \ominus]$. Therefore, the use of $[0°, 0°, 180°, 180°]$ excitation

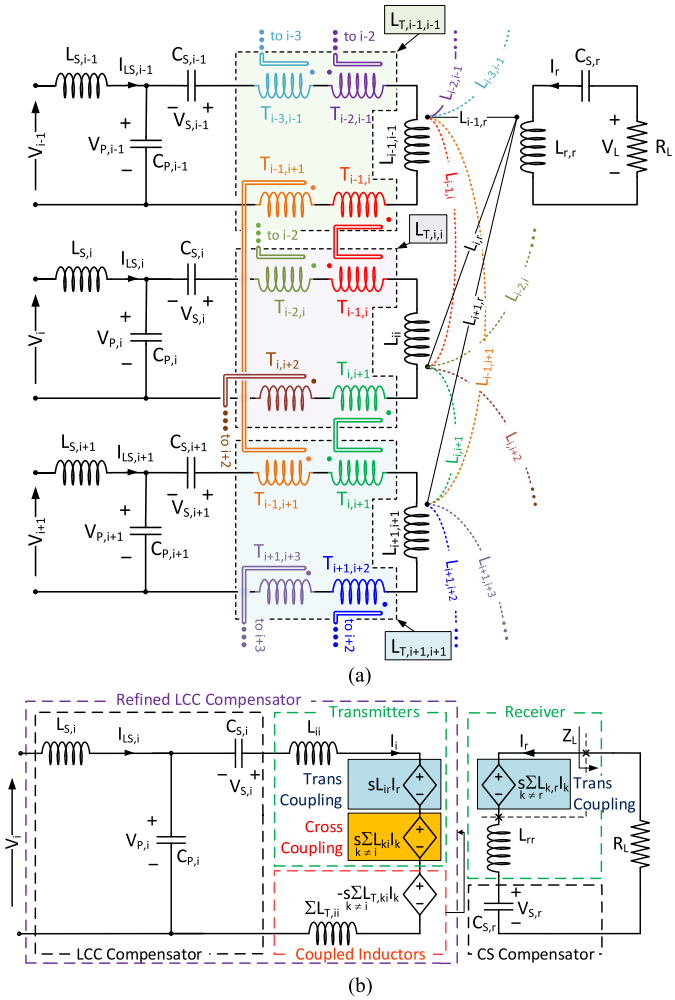

Fig. 6. Circuit diagram showing an NLC supplying power through its refined LCC compensators to a series capacitor compensated pickup circuit. (a) Cross couplings and their compensation using three adjacent transmitters, $i-1$, i, and $i+1$ ($L_{\mathrm{T},ii}$ represents total self-inductances of coupled inductors in secondary loop of LCC. The coupled inductors are coupled by identical ferrites (double lines), and their specifications are given in Table I). (b) Equivalent circuit for the i^{th} transmitter.

will remove the undesirable effect of coils 1 and 3 and maintain a higher level of transferred power in the system. The scenario can be replicated for n number of closely spaced transmitters located in a line. Although using a two-transmitter DWPT system would come up with the same result, for clarity, here, a three-transmitter DWPT system is used for demonstrations.

Considering x as the displacement axis of the pickup along the track, and $x = 0$ cm the center point of the middle transmitter, as shown in Fig. 1, the magnetic profile of the system is symmetric about $x = 0$ cm, as shown in Fig. 5. Therefore, the current profile for the third transmitter is similar to the first transmitter mirrored along $x = 0$ cm, the same is true for the LCC primary loop currents. For clarity, the currents of the third transmitter and LCC primary loop are not shown in Figs. 7 and 8.

As for the leg currents, there are two types of legs in the system, lateral legs, i.e., leg 1 and leg n, and middle legs. Current in the lateral legs is $I_{\mathrm{LEG},1} = I_{\mathrm{LS},1}$ and $I_{\mathrm{LEG},n} = -I_{\mathrm{LS},n}$, and for the middle legs, it is $I_{\mathrm{LEG},i} = I_{\mathrm{LS},i} - I_{\mathrm{LS},i-1}$, where $1 < i < n$. Simulation and theoretical results for these currents

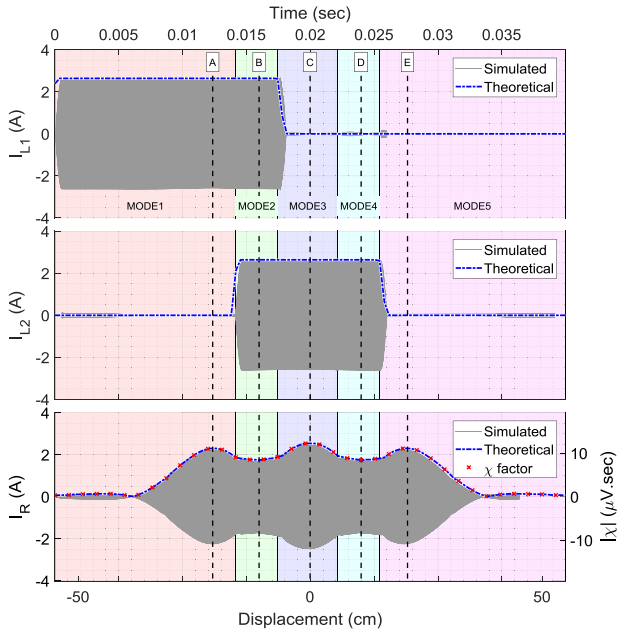

Fig. 7. Simulated and theoretical results for the currents of transmitters and receiver. The theoretical results are obtained from $I_i = -j\omega C_{\mathrm{P},i} V_{i,1}$ for the transmitter currents and (3b) for the receiver current.

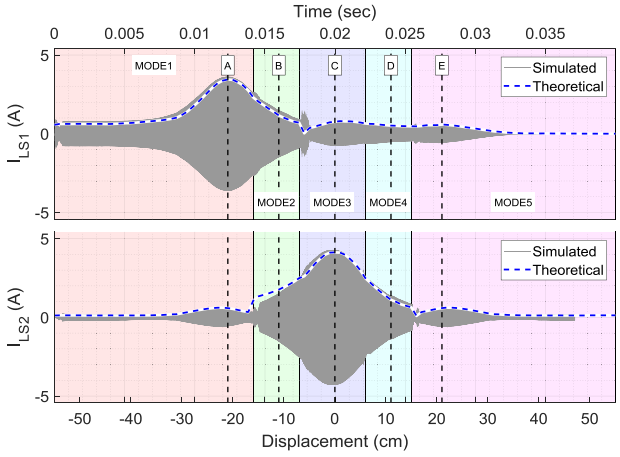

Fig. 8. Simulated and theoretical results for the LCC primary loop currents. The theoretical results are obtained from (4).

are shown in Fig. 9 for legs 1 and 2. Legs 3 and 4 have the same pattern as legs 2 and 1, respectively, except that they are mirrored along $x = 0$ cm. Therefore, they are not shown in the figure for clarity.

In (4), the quadrature components burden the power electronic switches with a severe hard switching, as they are 90° out of phase with V_i and disrupt zero current switching. To address this drawback, the work presented in [37] suggests a method to tune $C_{\mathrm{S},i}$ to compensate the undesirable effects of self-inductances, and the work presented in [22] uses coupled inductor to compensate the quadrature component of the induced voltage due to cross coupling.

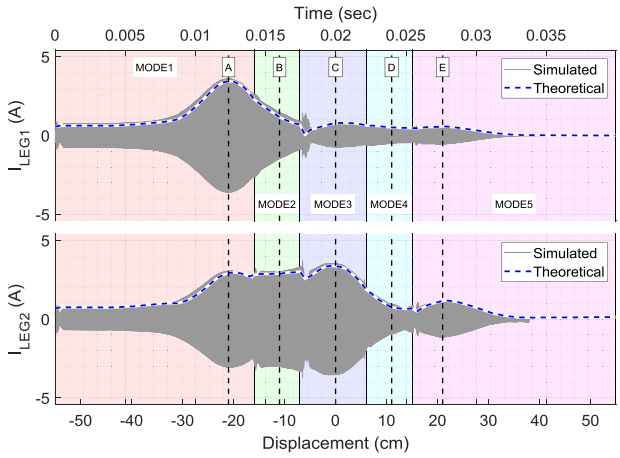

Fig. 9. Simulated and theoretical results for the LCC leg currents. The theoretical results are obtained by using (4) for the leg currents.

The coupled inductors approach is used in this article, as shown in Fig. 6, and they are tuned according to the following steps.

1) Find the cross couplings between the transmitters.
2) Design coupled inductors with a mutual inductance equal to the cross couplings.
3) Consider the effect of the primary and secondary self-inductances of coupled inductors in tuning the series capacitor of the LCC filter, based on the work done in [37].

To show how the refined LCC compensator helps the NLC with a desirable level of soft switching, simulation results shown in Fig. 10 compare converter leg currents feeding refined LCC compensator with that of unrefined LCC compensator at three different operational points of A, B, and C, which are shown in Figs. 5–9. The other operating points of D and E experience similar behavior as the system is symmetric about $x = 0$ cm.

As shown in Fig. 10, the refined LCC compensator can make a desirable level of soft switching in the proposed system at different positions of the pickup.

V. Mode Changing Strategy

In the operation of the proposed NLC, occurrence of electric transients is unavoidable as operational modes keep changing according to the position of the pickup. Unlike mechanical dynamics, which are due to the pickup displacement, changes in the NLC modes of operation can happen in a fraction of a second and they produce a high level of electrical transients in the track-side driving systems. The harsh electrical transients usually lead to the failure of power electronic switches and malfunctioning of some coils. Therefore, such transients must be mitigated through an appropriate method. Here, a simple ramping pattern is proposed as a strategy to gradually change the mode of operation based on position feedback as shown in Fig. 11(a).

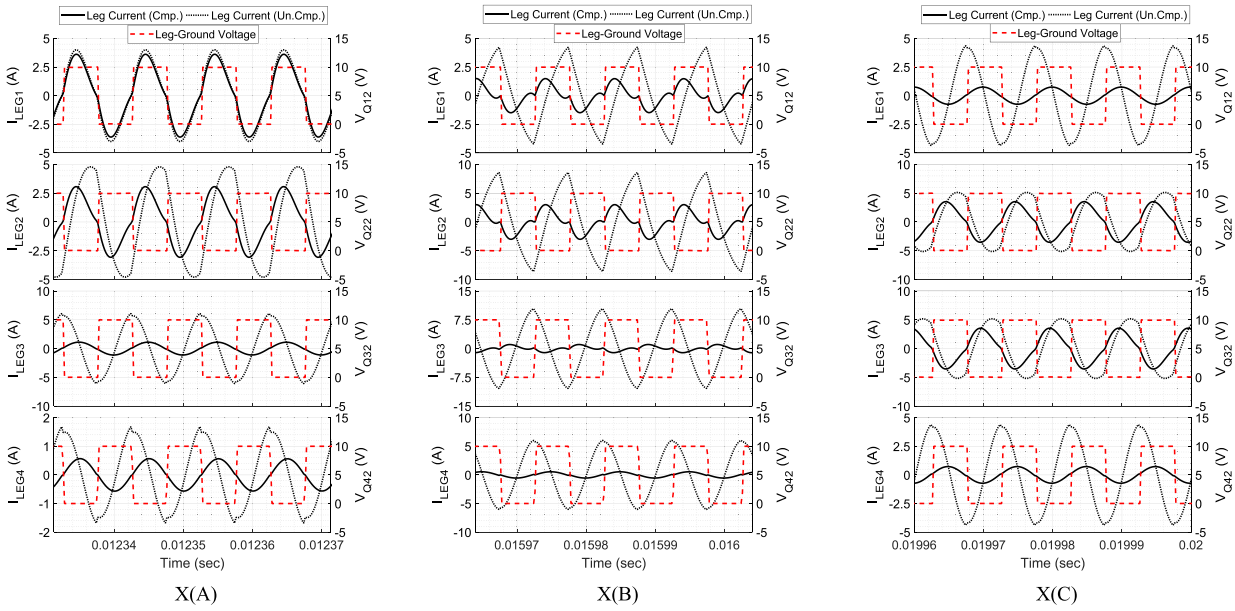

Fig. 10. Simulated leg currents for the refined LCC compensated system in solid black line and conventional LCC compensated system in dashed black line, which are compared with their corresponding leg-to-ground voltages for different positions of X(A), X(B), and X(C), shown in Fig. 5.

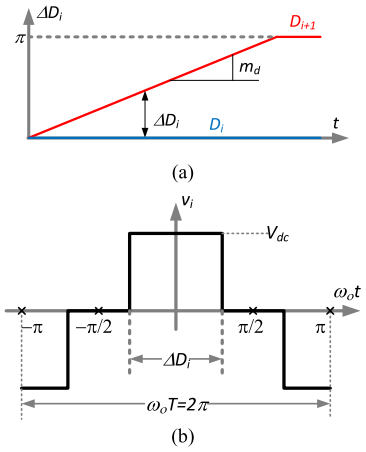

Fig. 11. Ramping strategy. (a) Ramping of angles between two adjacent legs and (b) generic NLC output voltage waveform.

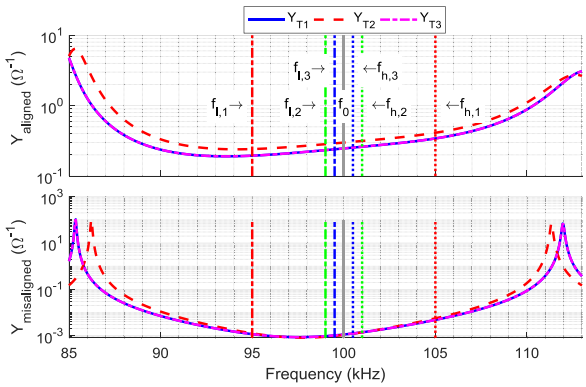

Fig. 12. Bifurcation phenomenon seen from the converter terminals at two effectively coupled (aligned) and weakly coupled (misaligned) positions. The dominant frequencies of the NLC output voltage waveform when it gradually ramps are shown in vertical lines for three different cases of $m_{d1}[f_{l,1}, f_{h,1}]$, $m_{d2}[f_{l,2}, f_{h,2}]$, and $m_{d3}[f_{l,3}, f_{h,3}]$.

To find an appropriate ramping slope, the effect of dominant harmonics in the input voltage while it changes from one pattern to another is investigated.

When the mode of operation changes, the phase angle between two adjacent legs varies. This can occur when either D_{i+1} or D_i changes. However, as $\Delta D_i = D_{i+1} - D_i = 180°$, simultaneous change in D_{i+1} and D_i results in a null voltage across the converter terminals when $D_{i+1}(t) = D_i(t)$ before they completely swap their angles.

Hence, to have a continuous flow of power during the transition, switching patterns are chosen so that only one leg changes its angle and get ramped. This change is not repetitive and cannot be described completely by Fourier-based analysis, such as double Fourier method. Therefore, short-time Fourier transform (STFT) is used to describe the behavior of the applied waveform to the segmented DWPT transmitters in frequency domain [38].

For this purpose, it is considered that $\Delta D_i(t = 0) = 0$ and it gradually increases to reach $\Delta D_i(t = \frac{\pi}{m_d}) = \pi$ with a rate of change of m_d, as shown in Fig. 11(b).

This behavior can be represented by (5), and its time-varying Fourier component is $a_n(t)$ in (6). However, the variation of ΔD_i is a piecewise function, and according to (6), $x(t)$ can be described as (7), where $0 \leq t < \frac{\pi}{m_d}$ is the window of STFT. After STFT calculations, the resulting frequency domain signal can be expressed as in (8)

$$\Delta D\,(t) = \begin{cases} m_d t; & 0 \leq t < \frac{\pi}{m_d} \\ \pi; & \frac{\pi}{m_d} \leq t \end{cases} \tag{5}$$

$$a_n\,(t) = \frac{2A}{n\pi} \sin\left(\frac{\Delta D\,(t)}{2}\right) \tag{6}$$

$$x(t)=\begin{cases}\sum_{n=1}^{\infty}\frac{2A}{n\pi}\sin\left(\frac{m_d t}{2}\right)\cos\left(n\omega_0 t\right); & 0\le t<\frac{\pi}{m_d}\\ \sum_{n=1}^{\infty}\frac{2A}{n\pi}\cos\left(n\omega_0 t\right); & \frac{\pi}{m_d}\le t\end{cases} \tag{7}$$

$$X(\omega)=\frac{A}{\pi}\sum_{n=1}^{\infty}\frac{1}{n}$$

$$\times\left\{\begin{array}{l}\left[\frac{\left(\frac{m_d}{2}+n\omega_0\right)}{\left(\frac{m_d}{2}+n\omega_0\right)^2-\omega^2}+\frac{\left(\frac{m_d}{2}-n\omega_0\right)}{\left(\frac{m_d}{2}-n\omega_0\right)^2-\omega^2}\right]+\\ \left[\begin{array}{l}\cos\left(n\omega_0\left(\frac{\pi}{m_d}\right)\right)\frac{j\omega}{(n\omega_0)^2-\omega^2}-\\ \sin\left(n\omega_0\left(\frac{\pi}{m_d}\right)\right)\frac{n\omega_0}{(n\omega_0)^2-\omega^2}\end{array}\right]e^{-j\frac{\pi}{m_d}\omega}-\\ \left[\begin{array}{l}\cos\left(\left(\frac{m_d}{2}+n\omega_0\right)\left(\frac{\pi}{m_d}\right)\right)\frac{\left(\frac{m_d}{2}+n\omega_0\right)}{\left(\frac{m_d}{2}+n\omega_0\right)^2-\omega^2}\\ +\sin\left(\left(\frac{m_d}{2}+n\omega_0\right)\left(\frac{\pi}{m_d}\right)\right)\frac{j\omega}{\left(\frac{m_d}{2}+n\omega_0\right)^2-\omega^2}\\ +\cos\left(\left(\frac{m_d}{2}-n\omega_0\right)\left(\frac{\pi}{m_d}\right)\right)\frac{\left(\frac{m_d}{2}-n\omega_0\right)}{\left(\frac{m_d}{2}-n\omega_0\right)^2-\omega^2}\\ +\sin\left(\left(\frac{m_d}{2}-n\omega_0\right)\left(\frac{\pi}{m_d}\right)\right)\frac{j\omega}{\left(\frac{m_d}{2}-n\omega_0\right)^2-\omega^2}\end{array}\right]e^{-j\frac{\pi}{m_d}\omega}\end{array}\right\}. \tag{8}$$

As it is obvious from (8), the oscillating frequencies are $\omega_{sb,h}=\frac{m_d}{2}+n\omega_0, \omega_{bb}=n\omega_0$, and $\omega_{sb,l}=\frac{m_d}{2}-n\omega_0$, known as higher sideband harmonics, baseband harmonics, and lower sideband harmonics, respectively. Following the same analogy, a similar result can be achieved for ramping with a negative slope.

These harmonics are responsible for triggering the oscillating natural frequencies of the system. On the other hand, bifurcation is a phenomenon that may be experienced in weakly coupled WPT systems, such as the proposed system in this article [15], [35]. This phenomenon bifurcates the natural oscillating frequency of the system into two. Consequently, bifurcation changes the natural response of the system. At bifurcated natural frequencies, the admittance seen from the NLC terminals is at its highest. Therefore, exciting the system near these frequencies results in a high flow of current and it can harm the components that are present in the current path, such as power electronic switches. Fig. 12 shows the admittance of the system from NLC terminals in logarithmic scale, when transmitters are fully coupled with the pickup (aligned) and when they are not coupled with the pickup (misaligned). In this figure, the baseband and sideband harmonics for three different slopes of ramping in ΔD_i, including $m_{d,1}=\frac{\omega_0}{20}$, $m_{d,2}=\frac{\omega_0}{100}$, and $m_{d,3}=\frac{\omega_0}{200}$, are shown. The higher and lower sideband harmonics are labeled, respectively, as f_h and f_l. According to Fig. 12 and (8), the lower the rate of change in ΔD_i, the closer the side band harmonics to the baseband harmonic, and the lower their effect on exciting bifurcated natural frequencies. This, however, may lead to an increase in time for mode changing, which is not desirable when the pickup moves fast.

As it is noticed from Fig. 12, the strength of coupling can change the sensitivity of the system when the mode changes. In other words, the coil which is coupled weaker is more vulnerable to mode changing transients (admittance peaks of misaligned

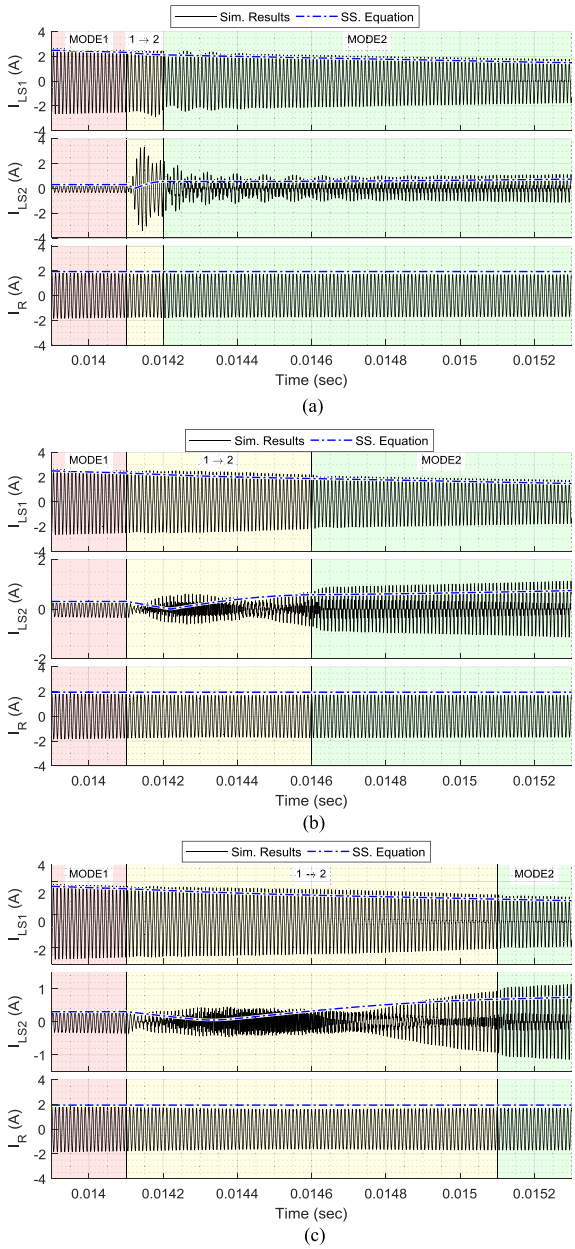

Fig. 13. Mode changing transients in the first and second LCC primary loop currents and the load current for three different cases of (a) m_{d1}, (b) m_{d2}, and (c) m_{d3}.

admittance in Fig. 12), and this can lead to failure in power electronic switches.

To see the effect of ramping at the given rates, the time domain transients in the first and second LCC primary loop currents and load current of the simulated system are shown in Fig. 13. This is carried out when the system mode of operation changes from "1" to "2."

Therefore, according to the trans couplings and admittance profiles, it is expected to see more severe transients in the second primary loop current than the first one. Fig. 13 also shows that the decrease in the rate of ramping from a steep rate of m_{d1} to lower rates of m_{d2} and then m_{d3} can effectively suppress the mode changing transients. Therefore, compared to other complex methods, such as feedback controllers, ramping can

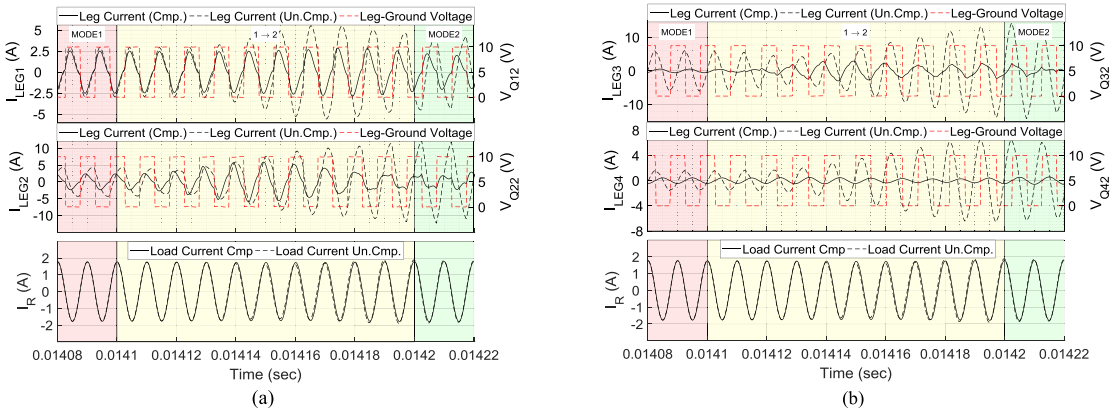

Fig. 14. Zoom-in of Fig. 13(a) to see the effect of transitions between two modes (while $\Delta D_1 = 180^\circ$ and ΔD_2 changes) on the (a) leg ("1" and "2") and load currents, and (b) leg ("3" and "4") with respect to the load current depicted in (a).

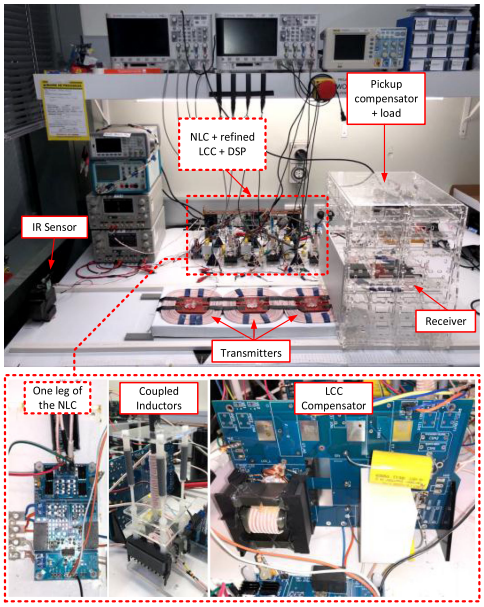

Fig. 15. Experimental setup of the NLC driving a closely spaced segmented DWPT system consisting of three transmitters and one receiver.

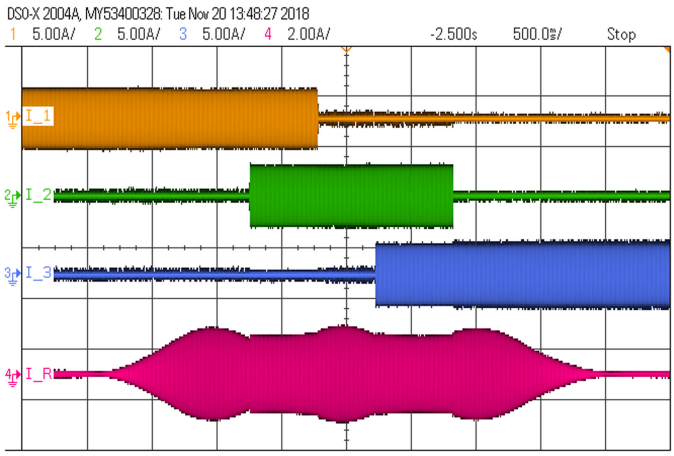

Fig. 16. Experimental results showing currents of the transmitters (I_1, I_2, and I_3) and receiver (I_r).

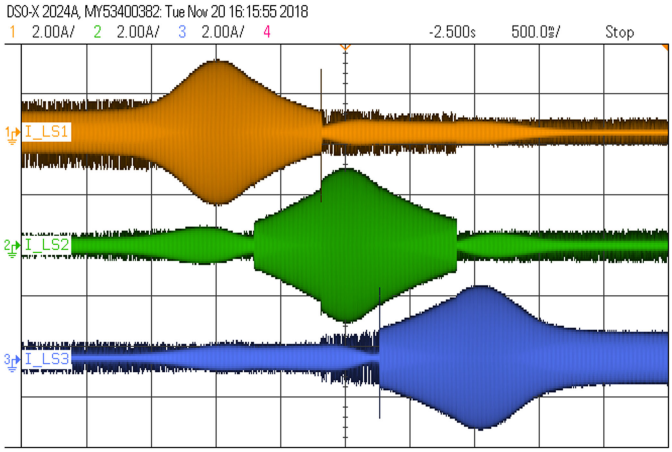

Fig. 17. Experimental results showing currents of the LCC primary loop for the transmitter compensators.

be seen as a simple and effective strategy in mitigating mode changing transients.

In terms of reliability, the simplicity of this pattern is one of its outstanding features, especially when it is used in a converter with several power electronic switches, such as the proposed NLC, as opposed to a complex control strategy, which would significantly decrease the reliability of the overall system.

It is worthy to mention that unlike the steady modes of operation (modes "1," "2," "3," and "4" in Figs. 5–9), during the transition between two consecutive modes, ΔD_i can vary and take values between 0° to 180°. Fig. 14 shows the zoom-in transition window of Fig. 13(a) for the first two legs and pickup currents, when the mode of operation changes from mode "1," $[\Delta D_1, \Delta D_2, \Delta D_3] = [180^\circ, 0^\circ, 0^\circ]$ to mode "2," $[\Delta D_1, \Delta D_2, \Delta D_3] = [180^\circ, 180^\circ, 0^\circ]$. As it can be seen in the period of transition, even though soft switching cannot be fully met, with the refined LCC compensator during this period (solid black line), the converter performance is better than the unrefined compensator (dashed black line), as shown in Fig. 14.

Moreover, LCC compensators have a high quality factor and it can help the cancelation of side band harmonics and transients. Therefore, as shown in Fig. 14, transmitter transients will not affect the load current.

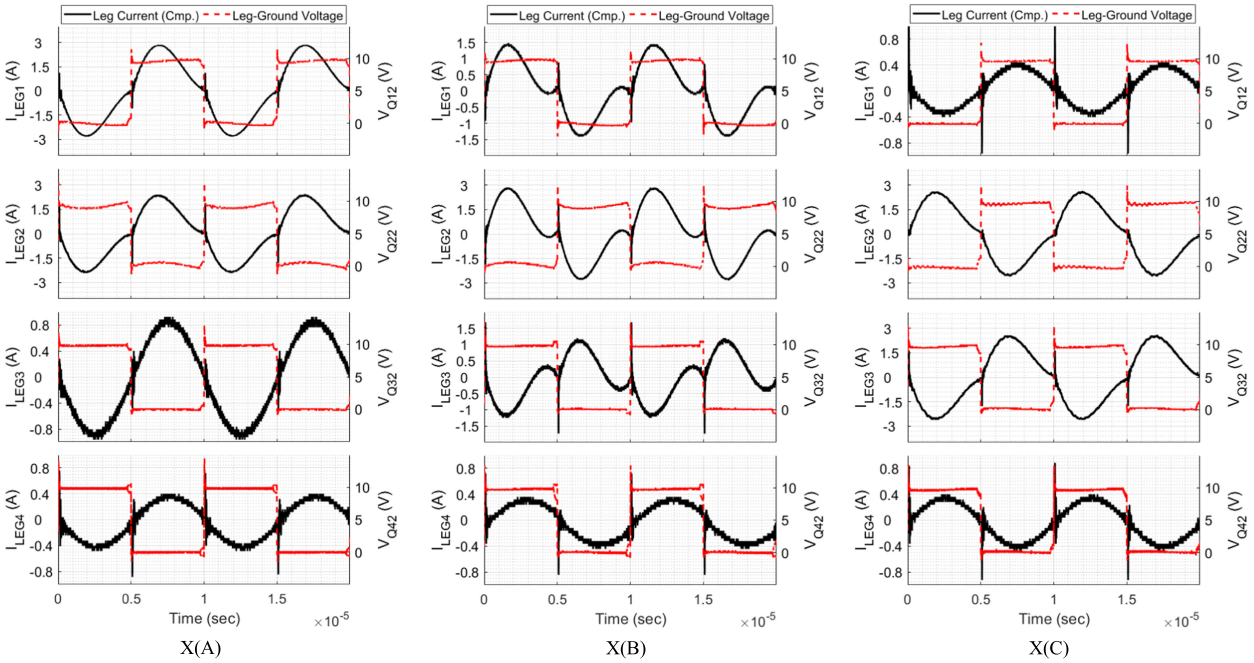

Fig. 18. Experimental results of the leg currents and leg-to-ground voltages at different positions of A, B, and C, shown in Fig. 5.

VI. Experimental Results

To validate the abstract concepts of the proposed expandable NLC to drive closely spaced segmented DWPT systems, a laboratory prototype is built based on the specifications given in Table I, as shown in Fig. 14. The experimental results are subsequently compared with the simulation results. The operation of the system when its pickup moves, soft switching at three different locations of A, B, and C, shown in Fig. 5, and the effect of ramping strategy on suppressing the mode changing transients are the topics that are focused in experimental results.

As shown in Fig. 15, the experimental setup consists of three transmitters and one receiver. To study the operation of the system, the pickup is moved at a constant speed of 22 m/s. The NLC is supplied by a 10 V power supply, which is filtered by a dc-link capacitive bank having three parallel 2200 uF electrolyte capacitors. The segmented DWPT transmitters are compensated by the refined LCC compensators augmented by coupled inductors.

Based on the trans couplings, shown in Fig. 5, the modes of operation and their margins are defined for the controller to drive the NLC. The currents of the transmitters and receiver while the pickup moves are shown in Fig. 16. LCC primary loop currents are also shown in Fig. 17. From the experimental results, it can be clearly seen that the current profiles and their behavior are consistent with the simulation results. In addition, similar to Fig. 10, leg-to-ground voltage and leg current of each leg are measured for positions A, B, and C, and they are shown in Fig. 18. From the results, it can be seen that soft switching is completely achieved for steady modes of operation.

To further investigate the effect of coupling inductors on the soft switching, the efficiency of the NLC and WPT coil compensator are measured when the system is compensated by the coupling inductors and they are compared with the uncompensated case as shown in Fig. 19. The measurements are carried

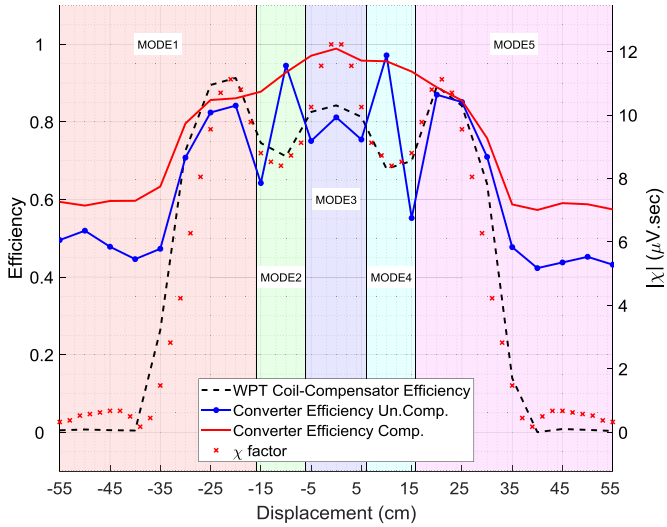

Fig. 19. Efficiency of the proposed converter when it is compensated by coupling inductors (red line), when each coil is independently compensated (starred blue line), and the efficiency of the WPT coil compensator when the converter is compensated by the coupling inductors (dashed black line).

out for 23 different positions, and they clearly show that using coupling inductors, the efficiency of the NLC can be significantly improved. To represent the efficiency using a single number, an effective range of DWPT is considered from $x = -30$ to 30 cm, and the average of efficiencies are taken during this range. The obtained efficiencies for the NLC equipped with the coupling inductors, and without the coupling inductors are found to be 0.912 and 0.803, respectively, which shows 13.6% of improvement in the converter efficiency with the use of coupling inductors.

Fig. 19 shows the efficiency of coil compensator in addition to the converter efficiency with and without coupling inductors. The figure also shows that there is a close relationship between

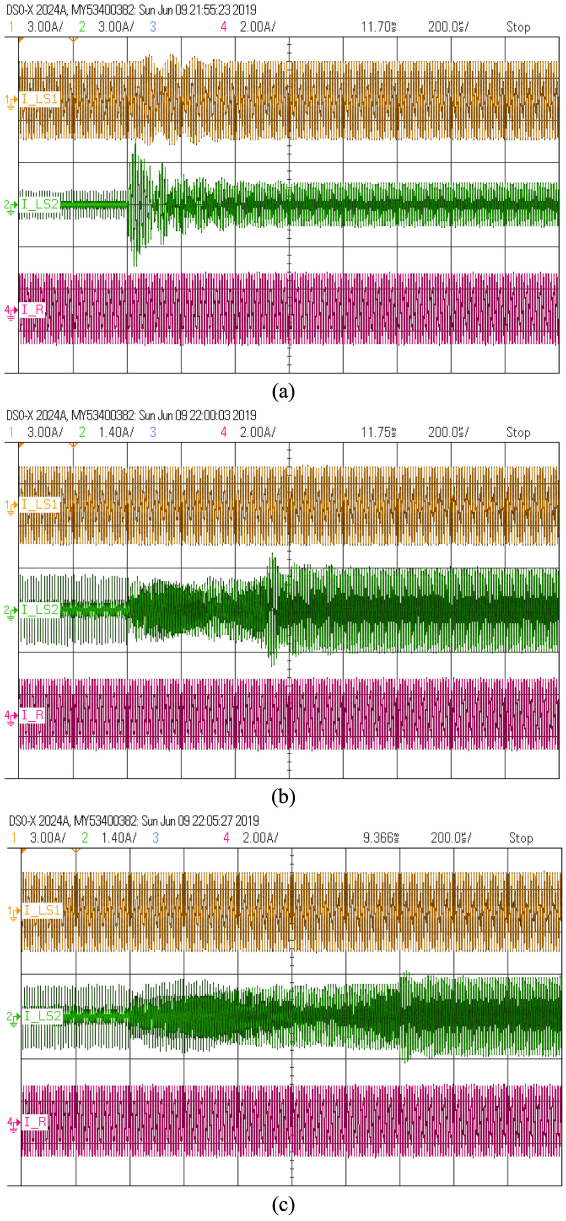

Fig. 20. Experimental results of mode changing transients in the first and second LCC primary loop currents and the load current for three different cases of (a) $m_{d1} = 314.16$ $k$rad/sec, (b) $m_{d2} = 69.813$ $k$rad/sec, and (c) $m_{d3} = 39.270$ $k$rad/sec.

the WPT coil compensator efficiency and the coordination factor, which emphasizes the importance of the coordination factor, stated in (3a), to optimize the coil efficiency.

Moreover, the proposed mode changing algorithm is experimentally investigated for the ramping rates of $m_{d1} = 314.16$ $k$rad/sec, $m_{d2} = 69.813$ $k$rad/sec, and $m_{d3} = 39.270$ $k$rad/sec, when the mode of operation is changed from "1" to "2." The mode changing experimental results for the first and second LCC primary loop currents and load current are shown in Fig. 20, and they are consistent with the simulated results shown in Fig. 13. Moreover, to show how the transition influences the load and two first primary LCC loop currents,

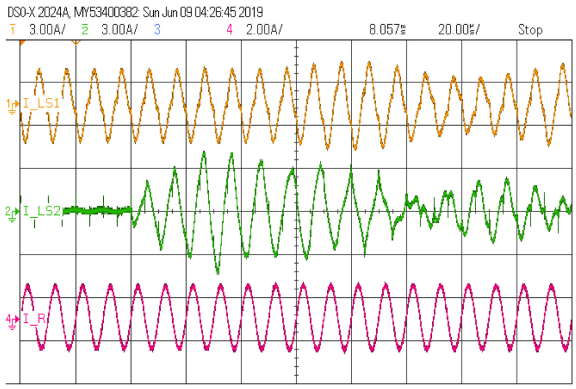

Fig. 21. Zoom-in view of transition in Fig. 20(a).

Fig. 21 shows a zoom-in view of Fig. 20(a) during the transition, and the results are compatible with the simulation results.

As discussed before, quick ramping, such as m_{d2}, tends to trigger bifurcated natural frequencies and will result in high level of transients. Moreover, due to being closer to the mechanical transients, low rate of ramping, such as m_{d3}, is not desirable. Therefore, ramping rate is set to 69.813 $k$rad/s, which is close to m_{d2}. Compared to mechanical transients, this rate of ramping is fast enough, and it can effectively suppress the mode changing transients. Therefore, the experimental results and simulation results show that the proposed methods are effective, reliable, and economical for dynamic wireless charging systems.

VII. Conclusion

In this article, a new expandable converter known as NLC is proposed to drive a multitransmitter WPT system for dynamic WPT chargers. Owing to the controllability of transferred power flow in each transmitter, it can prevent the null of power and make a flatter and steadier transferred power profile at different pickup positions. The proposed technique can reduce the number of coils and the volume of ferrite in the pickup side, and as such gives enormous economic benefits as those components are manufactured in mass. To make a uniform transferred power profile, the transmitters are positioned closely, and different modes of operation are defined for the NLC. As no currents flow through the noninteractive transmitters, there is a reduction in power losses. However, the proposed technique brings about the issues of cross coupling between transmitters and mode-changing transients. To address the undesirable effect of cross coupling on soft switching, a refined LCC compensator is proposed to maintain the soft switching regardless of the position of the pickup. In addition, a simple ramping strategy is used to suppress the mode changing transients. After analytically expressing the system, it is numerically simulated and experimentally tested, and the obtained results prove the credibility of the proposed techniques.

Appendix

The specifications of the simulated and built system are given in Table I. To have a better understanding about some geometric parameters, their dimensions are labeled in Fig. 22.

TABLE I
SIMULATION AND EXPERIMENTAL SPECIFICATIONS

Parameters	Values
Track ferrite length (cm)	TF= 60.9
Track transmitter(s) length (cm)	$[TT_1 = TT_2 = TT_3] = 20.3$
Pickup receiver width (cm)	TD = 19.5
Track coil expansion (mm)	$[TC_1 = TC_3 = TC_2] = 44$
Track transmitter number of turns	$[N_{T1} = N_{T2} = N_{T3}] = 16$
Pickup ferrite length (cm)	PF = 20.3
Pickup receiver length (cm)	PR = 20.3
Pickup receiver width (cm)	PD = 22
Pickup coil expansion (mm)	PC = 31
Pickup receiver(s) number of turns	$N_R = 11$
Ferrite thickness (mm)	t = 7
Pickup - track gap distance (cm)	G = 12.5
Ferrite relative permeability	2300 (N97)
Maximum of track self-inductance (uH)	$[L_{11} = L_{33}, L_{22}] = [92.2, 94.6]$
Maximum of track cross couplings (uH)	$[L_{12} = L_{23}, L_{13}] = [14, 5]$
Maximum of pickup self-inductance (uH)	$L_r = 53.9$
WPT frequency (kHz)	f = 100
Track LCC series inductor (uH)	$L_{si} = 7.67$
Track LCC parallel capacitor (nF)	$C_{pi} = 330$
Track LCC series capacitor (nF)	$C_{si} = [20.62]$
Coupled inductors self-inductance (uH)	$[L_{T1} = L_{T3}, L_{T2}] = [20, 17.6]$
Coupled inductors mutual inductances (uH)	$[L_{12}^* = L_{23}^*, L_{13}^*] = [14, 5]$
Coupled inductors relative permeability	2200 (ETD49-N87)
Pickup series capacitor (nF)	$C_{sr} = 47$
Pickup coil resistance (Ohm)	$R_{CP} = 0.076$
Transmitter coil resistance (Ohm)	$R_{CT} = 0.085$
Load (Ohm)	$R_L = 9$

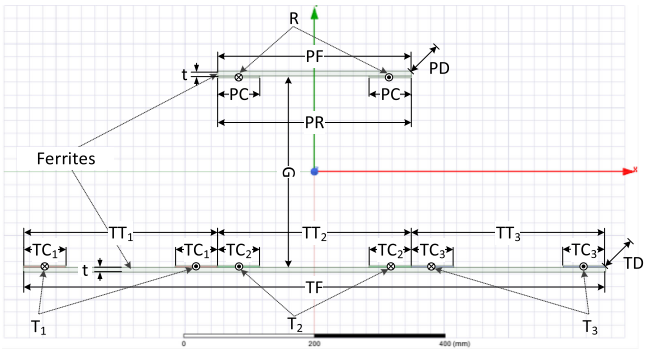

Fig. 22. Two-dimensional geometric representation of the segmented DWPT system.

REFERENCES

[1] N. P. Suh and D. H. Cho, *The On-line Electric Vehicle: Wireless Electric Ground Transportation Systems*. New York, NY, USA: Springer, 2017.

[2] G. R. Nagendra, G. A. Covic, and J. T. Boys, "Sizing of inductive power pads for dynamic charging of EVs on IPT highways," *IEEE Trans. Transp. Electrific.*, vol. 3, no. 2, pp. 405–417, Jun. 2017, doi: 10.1109/TTE.2017.2666554.

[3] A. Y. S. Lam, Y. Leung, and X. Chu, "Electric vehicle charging station placement: Formulation, complexity, and solutions," *IEEE Trans. Smart Grid*, vol. 5, no. 6, pp. 2846–2856, Nov. 2014, doi: 10.1109/TSG.2014.2344684.

[4] S. Li and C. C. Mi, "Wireless power transfer for electric vehicle applications," *IEEE J. Emerg. Sel. Topics Power Electron.*, vol. 3, no. 1, pp. 4–17, Mar. 2015, doi: 10.1109/JESTPE.2014.2319453.

[5] C. T. Rim and C. Mi, *Wireless Power Transfer for Electric Vehicles and Mobile Devices*. Hoboken, NJ, USA: Wiley, 2017.

[6] M. Budhia, J. T. Boys, G. A. Covic, and C. Y. Huang, "Development of a single-sided flux magnetic coupler for electric vehicle IPT charging systems," *IEEE Trans. Ind. Electron.*, vol. 60, no. 1, pp. 318–328, Jan. 2013, doi: 10.1109/TIE.2011.2179274.

[7] F. Musavi and W. Eberle, "Overview of wireless power transfer technologies for electric vehicle battery charging," *IET Power Electron.*, vol. 7, no. 1, pp. 60–66, Jan. 2014, doi: 10.1049/iet-pel.2013.0047.

[8] A. Khaligh and S. Dusmez, "Comprehensive topological analysis of conductive and inductive charging solutions for plug-in electric vehicles," *IEEE Trans. Veh. Technol.*, vol. 61, no. 8, pp. 3475–3489, Oct. 2012, doi: 10.1109/TVT.2012.2213104.

[9] M. Yilmaz, V. T. Buyukdegirmenci, and P. T. Krein, "General design requirements and analysis of roadbed inductive power transfer system for dynamic electric vehicle charging," in *Proc. IEEE Transp. Electrific. Conf. Expo.*, Jun. 2012, pp. 1–6, doi: 10.1109/ITEC.2012.6243497.

[10] S. Choi, J. Huh, W. Y. Lee, S. W. Lee, and C. T. Rim, "New cross-segmented power supply rails for roadway-powered electric vehicles," *IEEE Trans. Power Electron.*, vol. 28, no. 12, pp. 5832–5841, Dec. 2013, doi: 10.1109/TPEL.2013.2247634.

[11] K. Lee, Z. Pantic, and S. M. Lukic, "Reflexive field containment in dynamic inductive power transfer systems," *IEEE Trans. Power Electron.*, vol. 29, no. 9, pp. 4592–4602, Sep. 2014, doi: 10.1109/TPEL.2013.2287262.

[12] S. Zhou and C. C. Mi, "Multi-paralleled LCC reactive power compensation networks and their tuning method for electric vehicle dynamic wireless charging," *IEEE Trans. Ind. Electron.*, vol. 63, no. 10, pp. 6546–6556, Oct. 2016, doi: 10.1109/TIE.2015.2512236.

[13] Y. Guo, L. Wang, Q. Zhu, C. Liao, and F. Li, "Switch-on modeling and analysis of dynamic wireless charging system used for electric vehicles," *IEEE Trans. Ind. Electron.*, vol. 63, no. 10, pp. 6568–6579, Oct. 2016, doi: 10.1109/TIE.2016.2557302.

[14] J. Huh, S. W. Lee, W. Y. Lee, G. H. Cho, and C. T. Rim, "Narrow-width inductive power transfer system for online electrical vehicles," *IEEE Trans. Power Electron.*, vol. 26, no. 12, pp. 3666–3679, Dec. 2011, doi: 10.1109/TPEL.2011.2160972.

[15] W. Chwei-Sen, G. A. Covic, and O. H. Stielau, "Power transfer capability and bifurcation phenomena of loosely coupled inductive power transfer systems," *IEEE Trans. Ind. Electron.*, vol. 51, no. 1, pp. 148–157, Feb. 2004, doi: 10.1109/TIE.2003.822038.

[16] J. P. K. Sampath, D. M. Vilathgamuwa, and A. Alphones, "Efficiency enhancement for dynamic wireless power transfer system with segmented transmitter array," *IEEE Trans. Transp. Electrific.*, vol. 2, no. 1, pp. 76–85, Mar. 2016, doi: 10.1109/TTE.2015.2508721.

[17] J. M. Miller *et al.*, "Demonstrating dynamic wireless charging of an electric vehicle: The benefit of electrochemical capacitor smoothing," *IEEE Power Electron. Mag.*, vol. 1, no. 1, pp. 12–24, Mar. 2014, doi: 10.1109/MPEL.2014.2300978.

[18] O. C. Onar, J. M. Miller, S. L. Campbell, C. Coomer, C. P. White, and L. E. Seiber, "A novel wireless power transfer for in-motion EV/PHEV charging," in *Proc. 28th Annu. IEEE Appl. Power Electron. Conf. Expo.*, Mar. 2013, pp. 3073–3080, doi: 10.1109/APEC.2013.6520738.

[19] F. Lu, H. Zhang, H. Hofmann, and C. C. Mi, "A dynamic charging system with reduced output power pulsation for electric vehicles," *IEEE Trans. Ind. Electron.*, vol. 63, no. 10, pp. 6580–6590, Oct. 2016, doi: 10.1109/TIE.2016.2563380.

[20] A. Zaheer, H. Hao, G. A. Covic, and D. Kacprzak, "Investigation of multiple decoupled coil primary pad topologies in lumped IPT systems for interoperable electric vehicle charging," *IEEE Trans. Power Electron.*, vol. 30, no. 4, pp. 1937–1955, Apr. 2015, doi: 10.1109/TPEL.2014.2329693.

[21] Y. Tian, J. Tian, D. Li, and S. Zhou, "A multiple legs inverter with real time–reflected load detection used in the dynamic wireless charging system of electric vehicles," *Energies*, vol. 11, no. 5, pp. 1–20, 2018. [Online]. Available: https://www.mdpi.com/1996-1073/11/5/1275

[22] F. Farajizadeh, M. Vilathgamuwa, P. Jayathurathnage, G. Ledwich, and U. K. Madawala, "Soft switching in closely spaced multi-transmitter wireless power transfer systems," in *Proc. 45 Annu. Conf. Ind. Electron.*, Lisbon, Portugal, to be published.

[23] F. Farajizadeh, M. Vilathgamuwa, P. Jayathurathnage, and G. Ledwich, "Expandable N-legged converter for dynamic wireless power transfer," in *Proc. IEEE 18th Int. Power Electron. Motion Control Conf.*, Aug. 2018, pp. 115–120, doi: 10.1109/EPEPEMC.2018.8521754.

[24] A. Lusiewicz, J. Noeren, M. Jaksch, and N. Parspour, "A novel method for online coupling factor determination in inductive power transfer systems," in *Proc. IEEE Wireless Power Transfer Conf.*, Jun. 2018, pp. 1–4, doi: 10.1109/WPT.2018.8639460.

[25] S. Li and S. Y. R. Hui, "Comparative study on front-end parameter identification methods for wireless power transfer without wireless communication systems," in *Proc. Int. Power Electron. Conf. (IPEC-Niigata 2018 -ECCE Asia)*, 2018, pp. 2552–2557, doi: 10.23919/IPEC.2018.8507669.

[26] M. Khalilian, S. G. Rosu, V. Cirimele, P. Guglielmi, and R. Ruffo, "Load identification in dynamic wireless power transfer system utilizing current injection in the transmitting coil," in *Proc. IEEE Wireless Power Transfer Conf.*, May 2016, pp. 1–4, doi: 10.1109/WPT.2016.7498793.
[27] Y. Shin, K. Hwang, J. Park, D. Kim, and S. Ahn, "Precise vehicle location detection method using a wireless power transfer (WPT) system," *IEEE Trans. Veh. Technol.*, vol. 68, no. 2, pp. 1167–1177, Feb. 2019, doi: 10.1109/TVT.2018.2885942.
[28] W. Han, K. T. Chau, C. Jiang, and W. Liu, "Accurate position detection in wireless power transfer using magnetoresistive sensors for implant applications," *IEEE Trans. Mag.*, vol. 54, no. 11, pp. 1–5, Nov. 2018, doi: 10.1109/TMAG.2018.2843796.
[29] K. Hwang, J. Cho, J. Park, D. Har, and S. Ahn, "Ferrite position identification system operating with wireless power transfer for intelligent train position detection," *IEEE Trans. Intell. Transp. Syst.*, vol. 20, no. 1, pp. 374–382, Jan. 2019, doi: 10.1109/TITS.2018.2797991.
[30] ANSYS Electronics\Maxwell, 2016. [Online]. Available: https://ansyshelp.ansys.com/account/secured?returnurl=/Views/Secured/Electronics/v180/home.htm%23
[31] MATLAB, 2017. [Online]. Available: https://au.mathworks.com/downloads/
[32] R. Johari, J. V. Krogmeier, and D. J. Love, "Analysis and practical considerations in implementing multiple transmitters for wireless power transfer via coupled magnetic resonance," *IEEE Trans. Ind. Electron.*, vol. 61, no. 4, pp. 1774–1783, Apr. 2014, doi: 10.1109/TIE.2013.2263780.
[33] F. Kong, "Coil misalignment compensation techniques for wireless power transfer links in biomedical implants," M.S. thesis, Rutgers The State University of New Jersey, MI, USA, 2015.
[34] J. Hou, Q. Chen, Z. Zhang, S. C. Wong, and C. K. Tse, "Analysis of output current characteristics for higher order primary compensation in inductive power transfer systems," *IEEE Trans. Power Electron.*, vol. 33, no. 8, pp. 6807–6821, Aug. 2018, doi: 10.1109/TPEL.2017.2755862.
[35] W. Zhang and C. C. Mi, "Compensation topologies of high-power wireless power transfer systems," *IEEE Trans. Veh. Technol.*, vol. 65, no. 6, pp. 4768–4778, Jun. 2016, doi: 10.1109/TVT.2015.2454292.
[36] J. Meins, G. Buhler, R. Czainski, and F. Turki, "Contactless inductive power supply," in *Proc. 19th Int. Conf. Magn. Levitated Syst. Linear Drives*, Sep. 2006, pp. 527–535.
[37] Z. Pantic, S. Bai, and S. M. Lukic, "ZCS LCC-compensated resonant inverter for inductive-power-transfer application," *IEEE Trans. Ind. Electron.*, vol. 58, no. 8, pp. 3500–3510, Aug. 2011, doi: 10.1109/TIE.2010.2081954.
[38] K. Gröchenig, "The short-time Fourier transform," in *Foundations of Time-Frequency Analysis*. Boston, MA, USA: Birkhäuser, 2001, pp. 37–58.

Farzad (Farajizadeh) Farajizadeh (S'14) received the B.S. degree in electrical engineering from the Azad University of Gonabad, Gonabad, Iran, in 2009, and the M.S. degree in electrical engineering from the Azad University of Tehran, Tehran, Iran, in 2010. He is currently working toward the Ph.D. degree at the Queensland University of Technology, Brisbane, QLD, Australia.

His current research interests include wireless power transfer systems, power electronic converters, machine drives, FACTs, and renewable energy conversion.

D. Mahinda Vilathgamuwa (S'90–M'93–SM'99) received the B.Sc. degree in electrical engineering from the University of Moratuwa, Moratuwa, Sri Lanka, in 1985, and the Ph.D. degree in electrical engineering from Cambridge University, Cambridge, U.K., in 1993.

He joined the School of Electrical and Electronic Engineering, Nanyang Technological University, Singapore, in 1993. He is currently a Professor of power engineering with the Queensland University of Technology, Brisbane, QLD, Australia. He has authored/coauthored more than 300 research papers in refereed journals and conferences. His research interests include wireless power, power electronic converters, battery storage, and electromobility.

Dr. Vilathgamuwa is an Associate Editor for the IEEE TRANSACTIONS ON INDUSTRIAL ELECTRONICS.

Dejan P. Jovanovic (M'05) received the B.Sc. (Dipl. Ing.) degree in electrical and microelectronic engineering and the M.Sc. degree in systems control engineering from the University of Belgrade, Belgrade, Serbia, in 1996 and 2002, respectively, and the Ph.D. degree in statistics from the University of Queensland, Brisbane, QLD, Australia, in 2014.

He has held different positions both in industry and academia. He is currently with the Queensland University of Technology, as a Research Fellow within the power engineering group. His research interests include control systems, power electronics, and application of machine learning in fault diagnosis and fault-tolerant control.

Dr. Jovanovic won the IEEE 2005 Future Energy Challenge for a single-phase adjustable speed motor drive.

Prasad Jayathurathnage (S'12–M'17) received the B.Sc. degree in electronics and telecommunications engineering from the University of Moratuwa, Moratuwa, Sri Lanka, in 2009, and the Ph.D. degree in electrical and electronic engineering from the School of Electrical and Electronic Engineering, Nanyang Technological University, Singapore, in 2017.

He is currently a Postdoctoral Researcher with the Aalto University, Espoo, Finland. His research interests include high-frequency power converters, wireless power transfer, and biomedical implants.

Udaya K. Madawala (S'88–M'93–SM'06–F'18) received the B. Sc. degree (with Hons.) in electrical engineering from The University of Moratuwa, Moratuwa, Sri Lanka, in 1986 and the Ph.D. degree in power electronics from The University of Auckland, Auckland, New Zealand, in 1993.

In 1997, he joined the Department of Electrical and Computer Engineering, University of Auckland, where he is currently a Full Professor and focuses on a number of power electronics projects related to wireless grid integration of EVs for V2G applications and renewable energy.

Dr. Madawala is a Distinguished Lecturer of the IEEE Power Electronic Society and has served both the IEEE Power Electronics and Industrial Electronics Societies in numerous roles, relating to editorial, conference, advisory and technical committees, and chapter activities. He is currently an Associate Editor for the IEEE TRANSACTIONS ON POWER ELECTRONICS, and a member of both the Administrative Committee and Membership Development Committee of the IEEE Power Electronics Society.

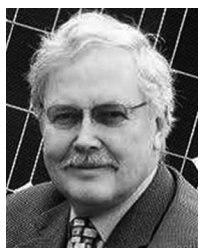

Gerard Ledwich (SM'89) received the Ph.D. degree in electrical engineering from the University of Newcastle, Newcastle, NSW, Australia, in 1976.

He is a Research Professor of Electric Power with the School of Electrical Engineering and Computer Science, Queensland University of Technology, Brisbane, QLD, Australia. His research interests include power systems, power electronics, and wide area control of smart grid.